Received: 13 July 2020 | Revised: 15 December 2020 | Accepted: 16 December 2020

DOI: 10.1111/joa.13393

Journal of Anatomy ANATOMICAL SOCIETY WILEY

ORIGINAL PAPER

Ontogenetic and *in silico* models of spatial-packing in the hypermuscular mouse skull

Nathan S. Jeffery[1] | Dylan C. Sarver[2,3] | Christopher L. Mendias[2,4]

[1]Institute of Life Course & Medical Sciences, University of Liverpool, Liverpool, UK

[2]Department of Orthopaedic Surgery, University of Michigan, Ann Arbor, MI, USA

[3]School of Medicine, Johns Hopkins University, Baltimore, MD, USA

[4]HSS Research Institute, Hospital for Special Surgery, New York, NY, USA

Correspondence
Nathan S. Jeffery, Institute of Life Course & Medical Sciences, University of Liverpool, Liverpool, UK.
Email: njeffery@liverpool.ac.uk

Abstract

Networks linking single genes to multiple phenotypic outcomes can be founded on local anatomical interactions as well as on systemic factors like biochemical products. Here we explore the effects of such interactions by investigating the competing spatial demands of brain and masticatory muscle growth within the hypermuscular myostatin-deficient mouse model and in computational simulations. Mice that lacked both copies of the myostatin gene (-/-) and display gross hypermuscularity, and control mice that had both copies of the myostatin gene (+/+) were sampled at 1, 7, 14 and 28 postnatal days. A total of 48 mice were imaged with standard as well as contrast-enhanced microCT. Size metrics and landmark configurations were collected from the image data and were analysed alongside *in silico* models of tissue expansion. Findings revealed that: masseter muscle volume was smaller in -/- mice at day 1 but became, and remained thereafter, larger by 7 days; -/- endocranial volumes begin and remained smaller; -/- enlargement of the masticatory muscles was associated with caudolateral displacement of the calvarium, lateral displacement of the zygomatic arches, and slight dorsal deflection of the face and basicranium. Simulations revealed basicranial retroflexion (flattening) and dorsal deflection of the face associated with muscle expansion and abrogative covariations of basicranial flexion and ventral facial deflection associated with endocranial expansion. Our findings support the spatial-packing theory and highlight the importance of understanding the harmony of competing spatial demands that can shape and maintain mammalian skull architecture during ontogeny.

KEYWORDS
endocranial, masseter, mouse, myostatin, spatial-packing

1 | INTRODUCTION

Anatomical structures physically interact to varying degrees throughout ontogeny, adulthood, and evolution. During ontogeny, genetically mediated changes in one structure can simultaneously affect important epigenetic changes in several surrounding structures. Moreover, interactions that reliably generate the same or similar phenotypes over successive ontogenies can shield from selection mutations in genes that would have otherwise defined those traits (see Green et al., 2017; Lahti et al., 2009; Zheng et al., 2019). These mutations can then accumulate, leading to punctuated phenotypic diversification as conditions prevail that destabilise the protective network of interactions and expose the gene variants to selection (Gould, 2002; Laland et al., 2015). Interactions also allow for phenotypic adjustments during life, which can accommodate behavioural changes of, for example, dietary niche or physical activity (e.g. Anderson et al., 2014). This capability extends into adulthood and can help genetically similar individuals and populations to tolerate and thrive under different environmental conditions (see Murren et al, 2015). The premise that structural interactions help define and maintain morphological outcomes has a long history and has taken many forms

over the decades (e.g. Kappers, 1932; Neubauer, 1925; Weidenreich, 1941; Weiss, 1933; Wolff, 1893). Most relevant to this paper are paradigms that define specific, typically spatially co-ordinated networks of interactions such as the functional matrix hypothesis formulated by Moss (Moss & Young, 1960) and its derivative, the spatial-packing hypothesis popularised by Ross (Ross & Ravosa, 1993). More recently, the concept has also become implicit to theories of morphological integration and modularity (e.g. Goswami et al., 2015; Klingenberg, 2014). Here we explore the spatial-packing hypothesis.

The central tenet of the spatial-packing hypothesis is that the head has a finite capacity to accommodate and maintain the functional integrity of a range of structures. Once spatially optimised, any subsequent relative expansion of one structure necessitates changes of form or function of one or more of its neighbouring structures. Lesciotto and Richtsmeier (2019) offer an excellent comprehensive review of the core principles (see also Lieberman et al., 2000; Singleton, 2013). Expansion of the brain is most often studied in this context, particularly amongst highly encephalised primates. There is substantial empirical evidence from adult interspecific studies and from the fossil record to support the notion that the primate skull, particularly the basicranium and face as well as the neurocranium, changed shape to fit relative expansion of the brain (e.g. Bastir et al., 2010; Ross & Henneberg, 1995; Ross & Ravosa, 1993). An often-cited competing spatial demand to brain expansion is the relative size of the masticatory apparatus. Biegert (1963) was first to outline this trade-off, suggesting that expansion of the masticatory apparatus relative to the brain constrains brain-related changes of the skull. Again, there is strong support from adult interspecific studies as well as the fossil record (e.g. Neaux et al., 2015; Ross & Henneberg, 1995; Ross & Ravosa, 1993; Veneziano et al., 2018). The mechanism(s) by which the skull responds to such competing spatial demands during ontogeny are unclear. It seems likely that strain gradients created by expanding tissues trigger cellular activity and incremental architectural remodelling (see Enlow, 1962 and, for example, more recently Edamoto et al., 2019). However, whilst the mechanotransduction of muscle and kinematic forces is well documented (see reviews by Stewart et al., 2020; Vincent & Wann, 2019), we know comparatively little about the efficacy of the low amplitude and low frequency stimuli elicited by tissue expansion. Another, congruent agent could be straightforward mechanical deformation – skull features are shaped and held in place by tissue growth in a way that is defined by the geometry, relative rigidity and spatial relationships of the tissues involved. This is reminiscent of the analogy popularised by Enlow (1976), and others, in which an inflating balloon bends around a piece of tape adhered to its surface.

Here we evaluate the potential of simple mechanical deformation to describe changes of skull shape and we also test Biegert's spatial-packing hypothesis using a myostatin (GDF-8) knock-out mouse model of hypermuscularity. Myostatin is a member of the transforming growth factor-beta (TGF-B) superfamily and acts as a negative regulator of skeletal muscle growth in vertebrates. It signals via type IB and IIB activin receptors to inhibit muscle progenitor cell proliferation, activate proteolytic systems and inhibit protein synthesis in the mature muscle. A loss of the gene encoding myostatin results in a greatly increased skeletal muscle mass, via fibre hypertrophy and hyperplasia (Mendias et al., 2006). Previous studies have shown significant increases of masseter mass among myostatin knock-out (-/-) mice in adults and at a range of ontogenetic time-points (e.g. Cray et al, 2011; Vecchione et al, 2010). Volumes reported by Jeffery and Mendias (2014) further confirmed masseter enlargement and revealed for the first time an associated reduction of brain size.

We use the latest advances of contrast-enhanced microCT, non-Euclidean geometric morphometrics as well as computational tissue modelling to test for shape changes that co-vary with enlargement of the masticatory muscles relative to brain size during ontogeny. Our spatial-packing hypothesis has two parts. The first part states that masticatory muscle enlargement constrains brain growth as implied by Stedman et al (2004) (see also Anthony, 1903). This predicts a close association between the ontogenetic timing of hypermuscularity and the reduced brain size seen in adult -/- mice. The second part follows Biegert's (1963) proposal that relative masticatory muscle enlargement constrains the effects of brain growth on the surrounding skull. This predicts that skull markers of brain expansion, such as base flexion and klinorhynchy (ventral facial deflection), are diminished among -/- mice. However, in our -/- mouse model the spatial-packing problem of enlarged musculature is conflated with reduced brain size, possibly due to suppressed myostatin expression within the brain (see Discussion), and with the structural effects of increased muscle and bite force (e.g. Byron et al., 2006; Williams et al, 2015). We therefore inferred the extricated and combined effects of brain and muscle growth on skull architecture *in-silico* and in doing so we also evaluate the ability of simple deformation to describe spatial-packing related phenomena. Simulations were evaluated empirically with reference to previously published observations notionally linked to spatial-packing. Predictions included: basicranial flexion and ventral facial deflection associated with simulated brain expansion (e.g. e.g. Ross & Ravosa, 1993); basicranial flattening and dorsal facial deflection (airorhynchy) associated with simulated muscle expansion (e.g. Ross & Henneberg, 1995); diminished basicranial flexion and diminished ventral facial deflection associated with simulated brain and muscle expansion (e.g. Biegert, 1963).

2 | METHODS

2.1 | Sample

Control (+/+) and myostatin deficient (-/-) mice on a C57BL/6 J background were reared and culled at the University of Michigan in strict accordance with Institutional Animal Care & Use Committee approval (PRO6079). Mice share a common maternal genotype and both sets of parents and offspring were reared under standardised laboratory conditions. A total of 48 male mice were sampled at 1, 7, 14 & 28 postnatal days (6 +/+ and 6 -/- per age group). Heads were removed postmortem and fixed in 10% neutral buffered formalin. Genotype of mice was determined by isolating DNA from tail biopsies and PCR-based

detection of the wild type *Mstn* (+) and knock-out *Mstn* (-) alleles as described by Mendias et al. (2006). Sex was confirmed using PCR probes against the *Sry* gene, which is located on the Y chromosome.

2.2 | Imaging

Each head was imaged twice. Once with standard microCT to capture the skull geometry and subsequently with I_2KI (9% w/v) enhanced microCT to visualise the muscle architecture (see Figure 1 and Jeffery et al, 2011). Both sets were acquired using a SkyScan 1272 (Bruker Ltd) with 50Kv, 200uA and an aluminium filter. Vertices of the resulting isometric voxels ranged from 26 to 40um. Contrast enhancement is associated with tissue shrinkage (Vickerton et al., 2013). The method was standardised here so the effect is likely to be the same for both groups and small given findings from similar whole mouse head studies (e.g. Baverstock et al., 2013; Cox & Jeffery, 2011; Jeffery & Mendias, 2014).

2.3 | Morphometrics

Masseter muscle and endocranial volumes were calculated using the stereological method implemented in VolumEst (v2010) for ImageJ (v1.51p). The endocranium is a reliable proxy for the brain in a range of craniates, including mammals (e.g. Dumoncel et al., 2020; Early et al., 2020). Relative masseter size was calculated as masseter volume divided by endocranial volume. Skull centroid size was calculated as the square root of the sum of squared distances between the landmarks shown in Figure 2a. Bivariate plots with local estimated scatterplot smoothing (LEOSS) and boxplots with Wilcoxon comparisons of -/- and +/+ means were created in R (version 3.6.2). Three-dimensional co-ordinates for a configuration of 18 reliable and readily identifiable skull landmarks (Figure 2a) were collected using the mark-up function in 3DSlicer (v4.10.1). This configuration was chosen to provide reasonable morphological representation whilst keeping the dimensionality of the shape space ($3L-7 = 47$) proportionate to the sample size (48) (see Bookstein, 2017, 2019; Cardini, 2019; Cardini et al, 2019). Geometric morphometric variations of the configuration of landmarks were investigated in MorphoJ (v1.07a) following the principles and methods outlined by Drake and Klingenberg (2008) and Klingenberg (2016). Allometric (size) related shape changes were investigated using a multivariate regression of symmetric Procrustes coordinates against log-transformed centroid size. Residuals from this regression were explored for nonallometric shape changes. Differences across age cohorts and experimental groups were evaluated in MorphoJ with Canonical Variate Analysis (CVA) and Discriminative Functions of Procrustes coordinates. Warped surfaces were created in Landmark (version 3.0) with reference to the co-ordinates generated by MorphoJ. For convenience, we illustrated the distribution of simulated forms within their own shape space using a Principal Components Analysis (PCA) of the covariance matrix and crossed checked findings against those generated by mesh deformations (see below).

2.4 | Computational simulation

Deformations of the skull due to endocranial and muscle enlargement were simulated *in-silico* using a mass exchange gradient

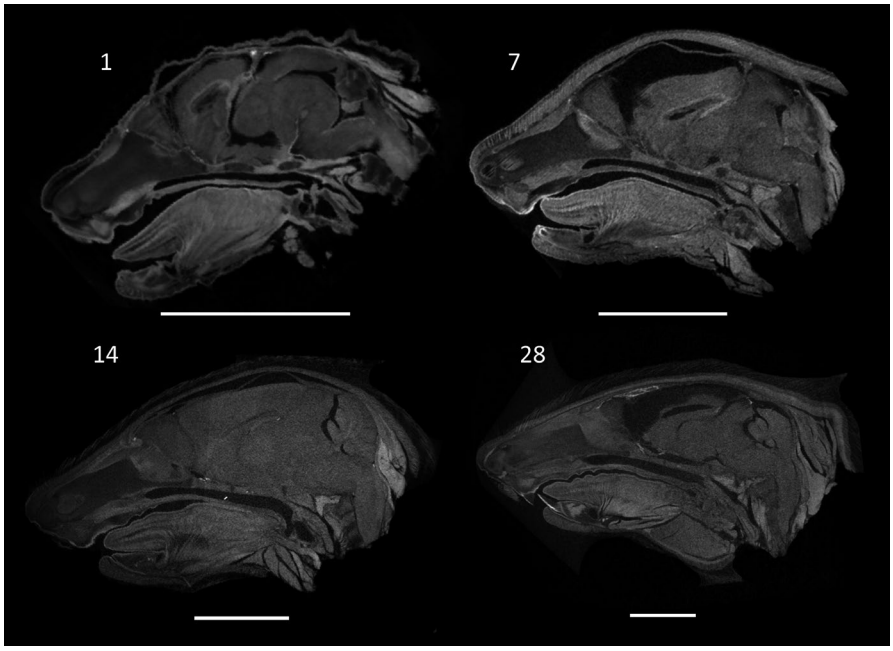

FIGURE 1 Example I_2KI enhanced microCT images reformatted along the midsagittal plane at postnatal day 1, 7, 14 and 28. Scale bar 5 mm

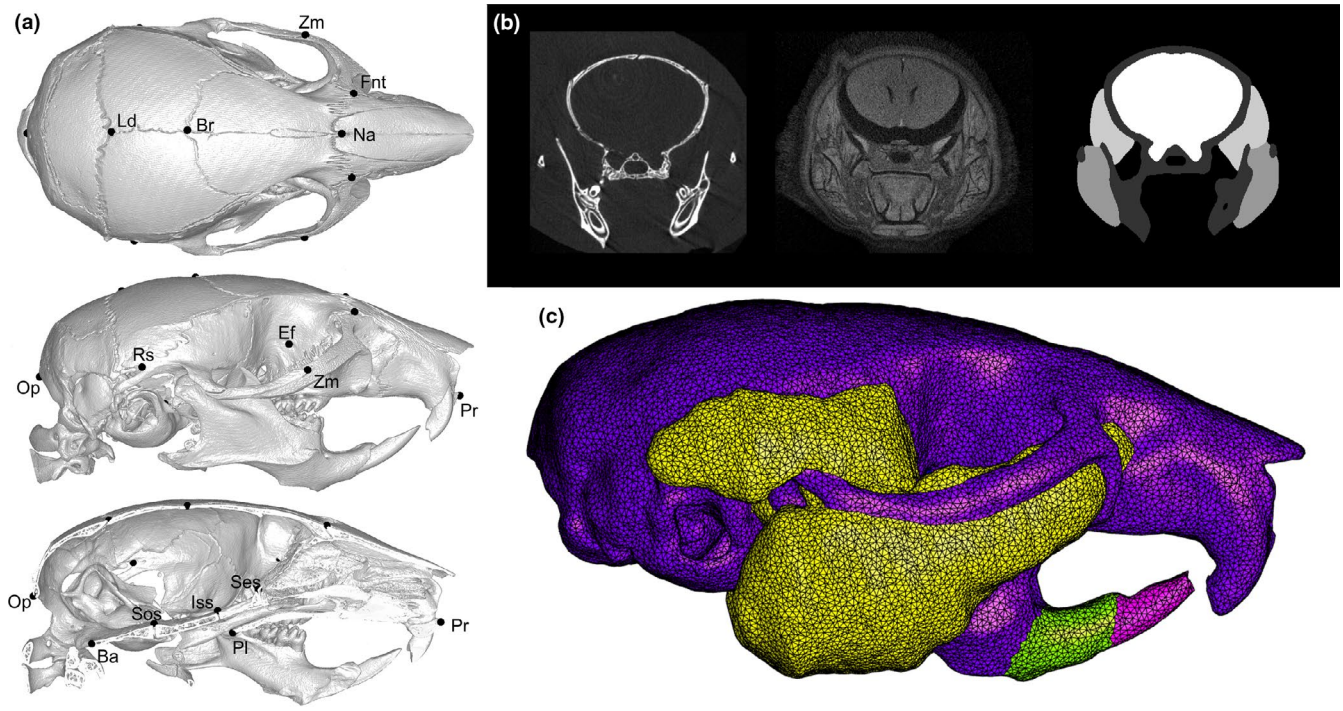

FIGURE 2 Reformatted and rendered image data showing: (a) from top to bottom, dorsal, lateral and midline views of the landmark configuration superimposed on 3D isosurfaces (Ba, basion; Br, bregma; Ef, ethmoid foramen; Fnt, junction between zygomatic, frontal and premaxillary bones; Iss, intersphenoidal synchondrosis; Ld, lambda; Na, nasion; Op, opisthion; Pl, posteriormost point of palatine suture; Pr, prosthion; Rs, recess above post-tympanic hook; Ses, spheno-ethmoidal synchrondrosis; Sos, spheno-occipital synchrondrosis; Zm, dorsal margin of zygomaticomaxillary suture); (b) from left to right, standard coronal microCT scan, I_2KI enhanced coronal microCT scan and the corresponding composite label mapping; (c) tetrahedral 3D mesh of mouse M1C1 used to create simulations (bone, purple; muscle, yellow; endocranium, not shown; green & pink, constraint)

finite element approach (see Ateshian et al, 2009). Co-registered standard and contrast enhanced microCT data (Figure 2b) for the control (+/+) 28-day mouse closest to the mean shape (specimen M1C1) were used to reconstruct, refine and mesh a model of the skull, mandible and masticatory muscles (masseter, temporalis and ptyergoids) in Amira version 5.4.1 (Thermo Fisher Scientific ltd, Waltham, Massachusetts, USA). The final decimated tetrahedral mesh, which consisted of 1.3 million elements (Figure 2c), was imported into FEBio version 2.8.2 (Maas et al., 2012) and parameterised. The simulation was simplified by assuming the skull was a structural continuum and that skull elasticity was invariant spatially as well as for the duration of the simulation. The mandibular incisors were used as rigid body constraints, and the mass exchange gradients representing constituent materials were adjusted to achieve the desired volumetric changes relative to the baseline +/+model ($S_{+/+}$). One model was created to simulate the 28 day -/- condition ($S_{-/-}$). In this case, the $S_{+/+}$ baseline model elastically deforms to accommodate a computationally driven 7% reduction of endocranial volume and 17% increase of masticatory muscle volume. This was repeated without the endocranial reduction (M_{+17}). The remaining simulations were used to explore shape changes associated with theoretical expansion of the muscles and endocranium (see Table 1). The models were solved using a nonlinear quasi-static method, landmarked and incorporated into the shape analyses as outlined above. Whole mesh deformations were also visualised in FEBio.

In all statistical comparisons a probability (p) value of ≤0.05 was used to identify the most prominent differences. Although

TABLE 1 Computationally driven changes of muscle and endocranial volume based on a 28-day control (+/+) mouse mesh

Simulation ID	Δ Muscle Volume %	Δ Endocranial Volume %
$S_{+/+}$	0	0
$S_{-/-}$	+17	−7
M_{+10}	+10	0
M_{+17}	+17	0
M_{+23}	+23	0
E_{+11}	0	+11
E_{+20}	0	+20
E_{+30}	0	+30
$M_{+6}E_{+5}$	+6	+5
$M_{+10}E_{+9}$	+10	+9
$M_{+27}E_{+21}$	+27	+21

$S_{+/+}$ and $S_{-/-}$ represent the +/+ and -/- conditions respectively. Remaining models simulate the combined and separate effects of muscle and endocranial expansion.

somewhat arbitrary and subject to recent criticism (e.g. Amrhein et al., 2019), this threshold was appropriate for the purposes of this study on the understanding that a $p > 0.05$ is not equivalent to no difference but can represent a weaker effect compared with ≤0.05.

3 | RESULTS

3.1 | Euclidean morphometrics

Bivariate plots against age with accompanying boxplots and Wilcoxon *p*-values are given in Figure 3a-d. Endocranial volumes were larger in +/+ mice from 1 through to 28 postnatal days (Figure 3a). Masseter volumes were at first larger among the +/+ mice (1 day), switching to larger among -/- mice at 7 and 28 days (Figure 3b). By 28 days -/- masseters and endocrania were on average 17% larger and 7% smaller, respectively. Both groups experienced increased relative masseter size (masseter volume/endocranial volume) after day 7 (Figure 3c). The increase was greater for -/- mice. There was little difference of centroid size until 28 days, at which point +/+ mice were on average 1.1 mm larger (Figure 3d). These findings predict corresponding shifts of skull form to accommodate relative masticatory muscle enlargement, and that such effects will be more pronounced among the -/- mice.

3.2 | Geometric morphometrics

Regression (Figure 4a) of the symmetric component of the Procrustes co-ordinates (combined fit; n = 48) suggests both -/- and +/+ mice followed a common allometric trend against centroid size, which explains approximately 77% of the total shape variation. Allometric changes from 1 to 28 days are illustrated in Figure 4b and included relative: elongation of the palate; narrowing of the midface and calvarium; flattening of the posterior cranial base and ventrodorsal shortening of the calvarium. Overall, the mean skull shape representative of all 28 day mice was relatively more compact and dolichocephalic while the face was longer and deflected dorsally (airorhynchy).

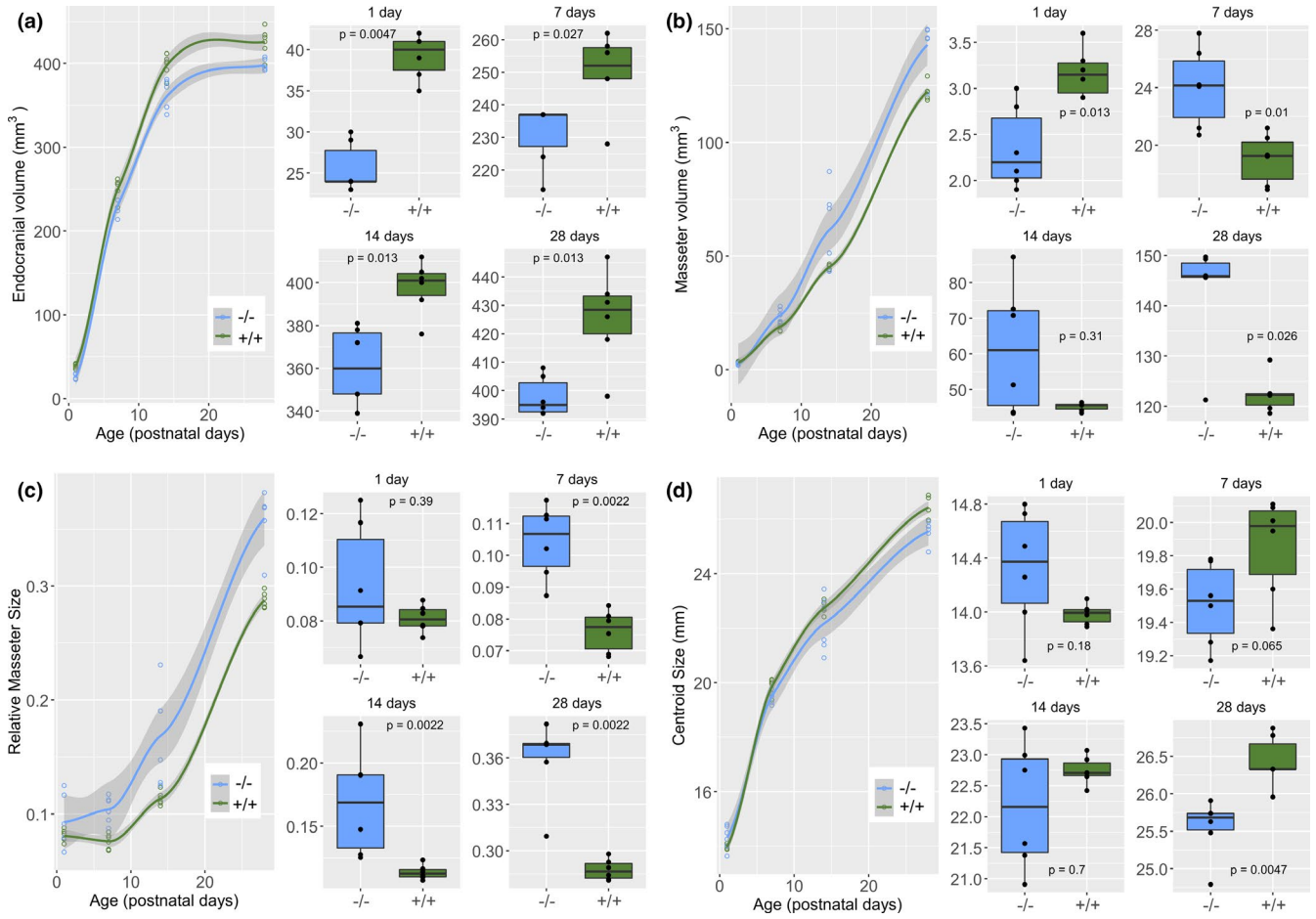

FIGURE 3 Bivariate plots with LEOSS fits against age (standard error, grey) and boxplot comparisons between +/+ (green) and -/- (blue) mice at 1, 7, 14 and 28 postnatal days for measures of (a) masseter volume; (b) endocranial volume; (c) relative masseter size (masseter volume/endocranial volume); (d) centroid size. Boxplots show the 25th, 50th & 75th percentiles with hinges for datum points within 1.5 times the percentile range (p-values are for Wilcoxon tests between +/+ and -/- means)

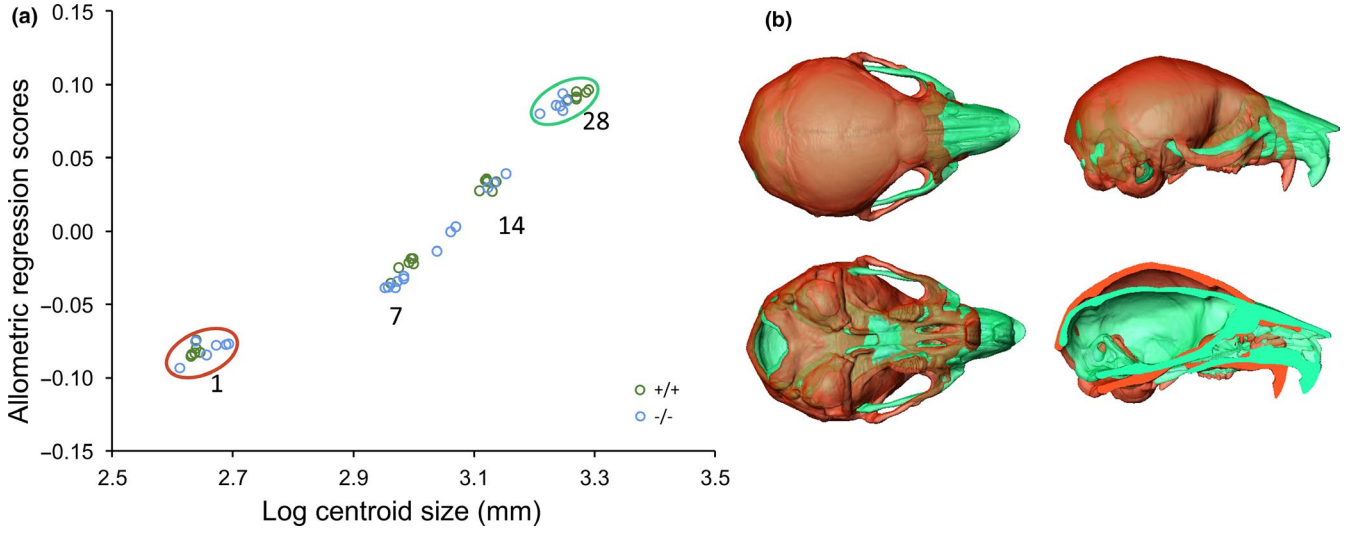

FIGURE 4 Size (allometric) related changes of craniofacial shape: (a) bivariate plot of regression scores from the Procrustes form space against log centroid size illustrating the common allometric trend through the age groups of -/- and +/+ mice; (b) surface renderings representing the allometric trend from the mean day 1 mouse shape (rose) to the mean day 28 shape (green)

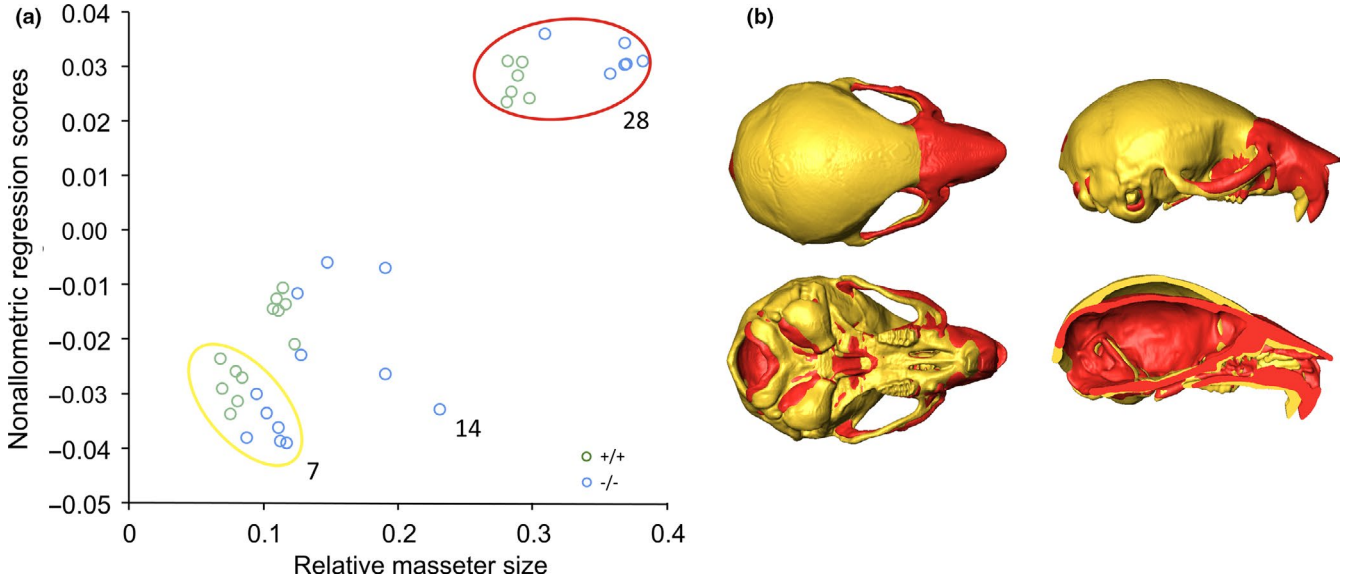

FIGURE 5 Size corrected (nonallometric) related changes of craniofacial shape in relation to relative masseter size from 7 to 28 days: (a) bivariate plot of nonallometric regression scores against relative masseter size, accounting for 48% of the size corrected shape variation; (b) surface renderings representing size corrected shape variation associated with increases of relative masseter size from 7 (yellow) to 28 days (red)

Relative masseter size predicted 59% (p-value <0.001) of the shape variation from 1 to 28 days. It also predicted 17% of the shape variance after size correction (residuals of regression against centroid size). Figure 3c suggested relative masseter enlargement occurred after day 1. Limiting the current analyses to days 7 to 28 showed that relative masseter size predicted 48% of the nonallometric shape variance (Figure 5a). Changes described included relative lateral displacement of the zygomatic arches, elongation of the face, as well as narrowing and ventrodorsal shortening of the neurocranium and slight dorsal bending of the face and of the posterior cranial base (Figure 5b). These patterns were broadly similar to the allometric shape changes shown in Figure 4b, reflecting shared groupings according to development (age) as well as growth (size).

Canonical Variate Analysis (CVA) of size corrected data revealed partitioning of the nonallometric shape space between -/- and +/+ mice across canonical variate 2, which represented 19% of the total variance (Figure 6a). Procrustes distances are given in Table 2. Shape differences at 28 days shown in Figure 5b were drawn from a discriminative function (Procrustes D = 0.0271, p = <0.0001; cross-validation 100% accurate assignment). The major shape differences were lateral displacement of the arches and caudolateral expansion of the neurocranium among the 28 day -/- mice. Also observed in

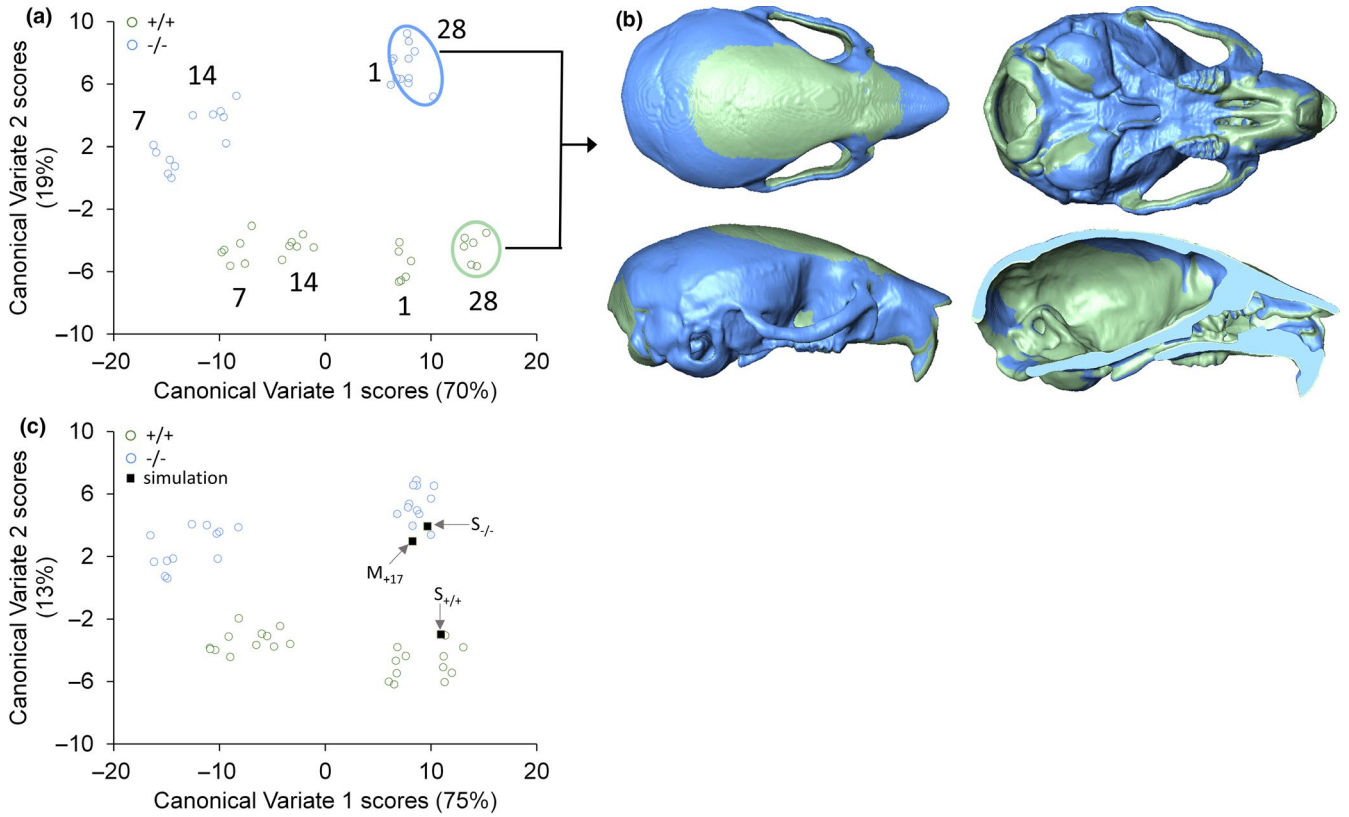

FIGURE 6 Nonallometric differences between -/- and +/+ mice: (a) Plot of canonical variate scores showing the partial separation of age groups along CV1 and separation of -/- & +/+ mice along CV2; (b) 3D renderings representing nonallometric shape differences between MSTN-/- and +/+ mice at day 28 based on a discriminative function; (c) plot of canonical variate scores including simulations (refer to Table 1 for abbreviations)

TABLE 2 Myostatin -/- versus +/+ canonical variate analysis (1000 permutations) based on size corrected Procrustes data

Age Grp (days)	N	Procrustes Distance †	Permutation *p*-value
1	12	0.0256	0.0101
7	12	0.0189	0.0008
14	12	0.0273	0.0014
28	12	0.0271	0.0020

† distance between +/+ and -/- mice.

-/- mice were a decrease in facial height, particularly around the rostrum, and slight dorsal deflection of the palate.

3.3 | Simulations

Computational simulations are summarised in Table 1. To evaluate our approach, the simulations of the control model ($S_{+/+}$) and those approximating the -/- condition at 28 days ($S_{-/-}$ & M_{+17}) were combined with the main dataset and the CVA reported above was repeated. Figure 6c shows the equivalent plot including the control simulation ($S_{+/+}$), which clusters with the 28 day +/+ mice. Shape differences described by the variates are the same in both analyses. The simulated 17% muscle expansion (M_{+17}) and muscle expansion plus 7% endocranial reduction ($S_{-/-}$) models both cluster with the -/- mice (please refer to Table 1 for abbreviations and conditions). These findings confirmed that simulations broadly mimic actual shape differences observed between -/- and +/+ mice (see above) and indicated that muscle enlargement rather than reduced endocranial growth had the greatest influence on these shape differences.

The three empirically informed simulations ($S_{+/+}$, $S_{-/-}$ & M_{+17}) were then combined with extended, theoretical, models of muscle and endocranial expansion (see Table 1) and subjected to PCA. PC1 explained 94% of variance (Figure 7a), representing mostly simulated increases of masticatory muscle volume in one direction (+PC) and simulated increases of endocranial volume in the other (-PC). Simulated enlargement of the masticatory muscles was associated with lateral displacement of the zygomatic arches, dorsal deflection of the face (airorhynchy), ventrodorsal shortening of the neurocranium and retroflexion (flattening) of the posterior cranial base (Figure 7b). The opposite trend was seen with simulated endocranial enlargement (Figure 7c), which was characterised by basicranial flexion, neurocranial enlargement and ventral deflection of the face (kyphosis or klinorhynchy). PC2 (6%) showed the combined effects of computationally driven muscle and endocranial expansion. Findings indicate that muscle expansion limits endocranial induced flexion of the posterior cranial base and endocranial expansion

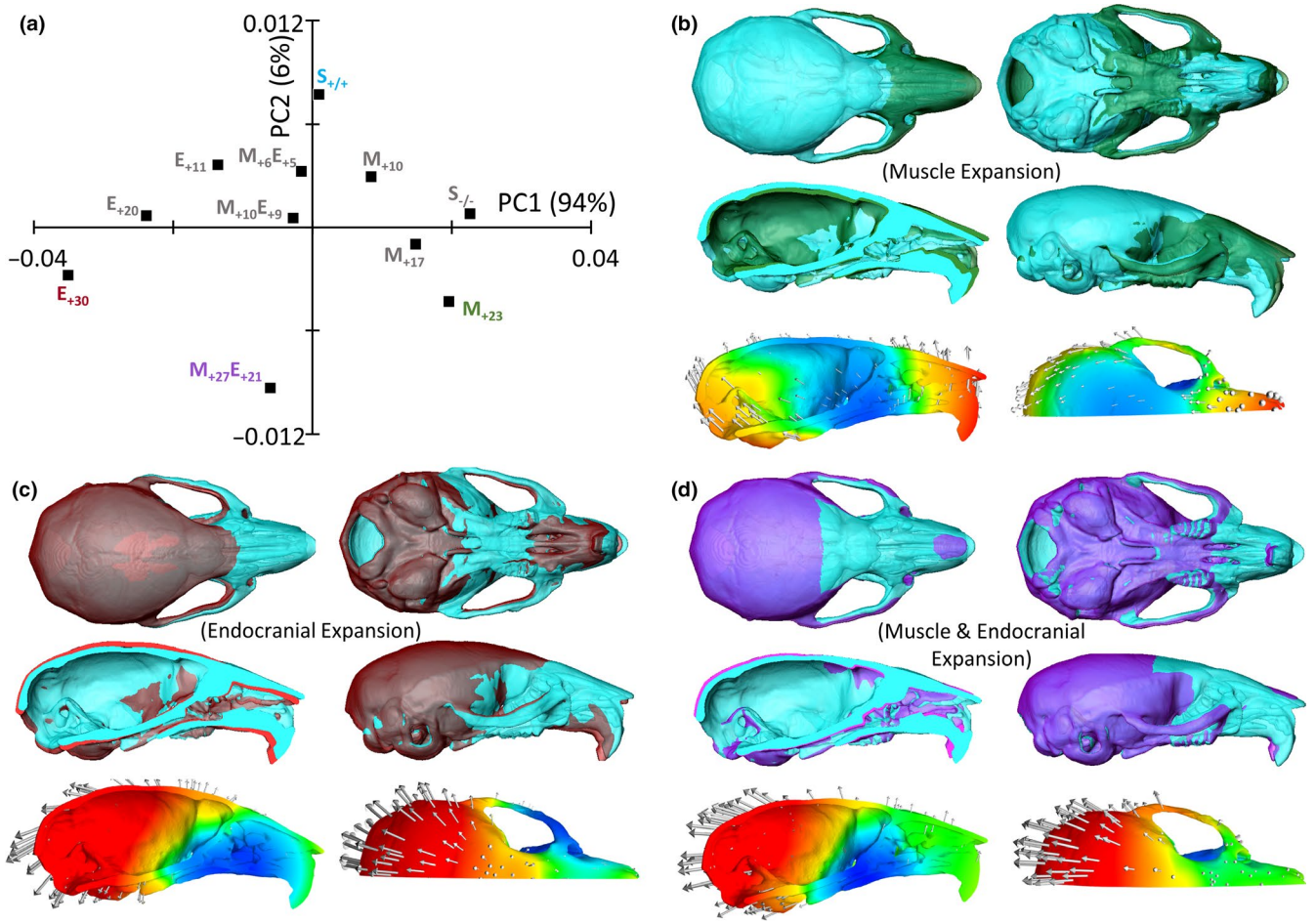

FIGURE 7 Soft-tissue expansion simulations; (a) plot showing the distribution of simulated skulls along principal components 1 and 2 of the shape space (refer to Table 1 for abbreviations). Note that simulated muscle (e.g. M_{+17}) expansions are primarily distributed along positive PC1 scores whereas simulated endocranial expansions (e.g. E_{+20}) fall along the negative PC1 scores. Combined muscle and endocranial expansions (e.g. $M_{+27}E_{+21}$) fall along PC2; (b-d) 3D renderings of the corresponding shape changes (+/- 0.05 PC scale factor) from the mean control shape ($S_{+/+}$, light blue) to the simulated shape: (b), green represents expanded muscle [M_{+23}]; (c), rose represents expanded endocranium [E_{+30}]; (d), purple represents combined expansion of muscle and endocranium [$M_{+27}E_{+21}$]). Accompanying colour mapped 3D renderings illustrate the corresponding mesh deformations (red, high deformation; blue, low deformation; arrows also indicate direction and magnitude [arrow length] of deformation)

limits dorsal deflection of the face associated with muscle enlargement (Figure 7d). Whole mesh (1.3 million elements) displacement vector plots (bottom row in Figure 7b-d) revealed similar trends to the above landmarked defined analyses. Endocranial expansion was primarily characterised by neurocranial expansion as well as ventral deflection of the face and the cranial base, including basicranial flexion (bottom row Figure 7c). By contrast, muscle expansion was primarily characterised by dorsal deflection of the posterior neurocranium, face and cranial base, including basicranial retroflexion, as well as lateral expansion of the zygomatic arches (bottom row Figure 7b). Combining the two simulated expansions appears to redirect and magnify the displacement posteriorly whilst constraining the flexion to basicranial elongation and the extent of dorsal facial deflection (bottom row Figure 7d). Lateral displacement of the zygomatic arches remained.

4 | DISCUSSION

Compared with the controls (+/+), the 28-day-old myostatin deficient (-/-) mice had on average 17% larger masseters and 7% smaller endocrania, the latter being used here as a proxy for brain size (see methods). A previous study by Jeffery and Mendias (2014) suggests this pattern continues into later adulthood with differences of +43% and −16%, respectively in mice aged 60 to 517 days (average 233 days). Similar increases in masseter size have been reported before (see Vecchione et al., 2007; 2010; Cray et al, 2011). In particular, our results corroborate those of Vecchione et al (2010) showing that day old +/+ mice have larger masseters than -/- mice. These findings suggest that the hypermuscular phenotype emerges after birth, during the first week of life, and then rapidly accelerates. By contrast, the -/- mice had smaller endocrania from day one, which suggests

the reduced brain size occurred in-utero and preceded and then accompanied the accelerated muscle growth. Thus, our findings do not corroborate the idea of muscularity directly constraining brain size as implied by Stedman et al (2004). Indeed, that -/- endocrania are smaller at birth suggests the involvement of more systemic factors.

Myostatin is known to be an important pre- and postnatal metabolic regulator (Carneiro et al, 2013; Guo et al, 2009; McPherron & Lee, 2002; Mouisel et al, 2014; Ploquin et al, 2012) and has been shown to act as a communicative link between muscle and fat (Deng et al, 2020; Kong et al, 2018). Deficiency may therefore limit the availability of lipids for myelin formation, which can in turn impede intra-uterine brain growth (Bourre et al., 1981; Morand et al., 1981). Myostatin deficiency may also have altered brain cell development. Since we reported the reduced endocranial phenotype in 2014, several studies have reported the abundant expression of myostatin-like proteins throughout the brain, including glia as well as neurons (e.g. Augustin et al., 2017; Hayashi et al., 2018; Schafer et al., 2019). This suggests myostatin is an important factor for neuronal growth and maintenance. We therefore contend that the reduced -/- endocrania reported here and by Jeffery and Mendias (2014) are the product of altered prenatal neuronal growth, possibly exacerbated by the metabolic demands of growing and maintaining larger muscles later in life.

Rather than constraining brain size, our mouse data and more clearly our simulations support the hypothesis that masticatory muscle enlargement limits the effects of brain expansion on the surrounding skull. Most notably, masticatory muscle enlargement curbs basicranial flexion, whilst brain enlargement in turn restricts some effects of muscle enlargement such as dorsal deflection of the face (Biegert, 1963; see also Ross & Ravosa, 1993; Ross & Henneberg, 1995). The aim of our computational approach was not to replicate the intricacies of the murine head but to simulate deformation driven by tissue expansion. Realism could and should be enhanced in future models, albeit at the expense of computational load and possibly stability. Refinements might include, for example, growth of additional anatomical modules such as the eyes and extraocular apparatus (e.g. Jeffery et al., 2007; Ross & Kirk, 2007), nuchal musculature and nasal turbinates as well as the face (Bastir et al., 2010), the pharynx (e.g. Jeffery, 2005) and the nasal septum (Jeffery et al., 2007). Adding ontogenetic shifts of skull compliance will be particularly enlightening, especially changes related to the formation of ossification centres and the subsequent localisation of deformation to, and eventual fusion of, sutures and synchondroses (see Jeffery & Spoor, 2004; Michejda, 1972; Oladipupo et al., 2020). While adding such complexity will no doubt provide more detail and nuance (see for example Lee & Richtsmeier, 2019), it is remarkable nonetheless how much of the *in-vivo* changes were captured here *in-silico* on the basis of simply tissue expansion and elastic deformation. Mechanical deformation appears to mirror the effects of mechanisms underlying ontogeny of the murine skull and is perhaps a precursor or adjunct to physiological tissue (re)modelling.

From these and previous findings, we can begin to infer the variegated and phasic nature of skull ontogeny (see also Bastir & Rosas, 2016; Zollikofer et al., 2017). We know that morphogenetic covariations predominate during embryogenesis. Presumably, these trends remain coherent for most of prenatal life, reflecting the residual power of the genes involved as well as relatively relaxed functional demands and spatial constraints. For example, consider the fetus suspended in amniotic fluid, nourished via the umbilical cord and with a flexible, membranous, calvarium. Recent in-utero MR images have also shown a comfortable margin of cerebrospinal fluid surrounding the brain, which could be displaced via arachnoid granulations to lessen the physical effects of encephalisation on the surrounding skull (see figures in Jarvis et al, 2019; Kyriakopoulou et al., 2017). In other words, the head is not yet spatially optimised at this stage and retains capacity to accommodate expanding tissues. However, as ontogeny proceeds, the genetic signals lose coherence, developmental noise accumulates and tissues become increasingly crowded and sculpted by functional demands like mastication. At this point, the established spatial arrangement of tissues, referred to here as heterotopy, would be distorted by greater competition for space as modules adopt distinct allometric trajectories and disperse along different heterochronic timelines (see Zelditch & Fink, 1996; Zollikofer & Ponce De León, 2004). This idea, which is summarised in Figure 8, might help explain why investigations of spatial-packing using fetal samples (e.g. Jeffery & Spoor, 2002; 2004; Jeffery, 2003; Jeffery et al., 2007) have seemingly contradicted adult studies (e.g. Neaux et al., 2015; Ross & Henneberg, 1995; Ross & Ravosa, 1993; Veneziano et al., 2018). Indeed, whilst it pains at least one of us (NJ) to concede, it appears that spatial-packing like phenomena are best detected later in ontogeny and possibly in differences among the

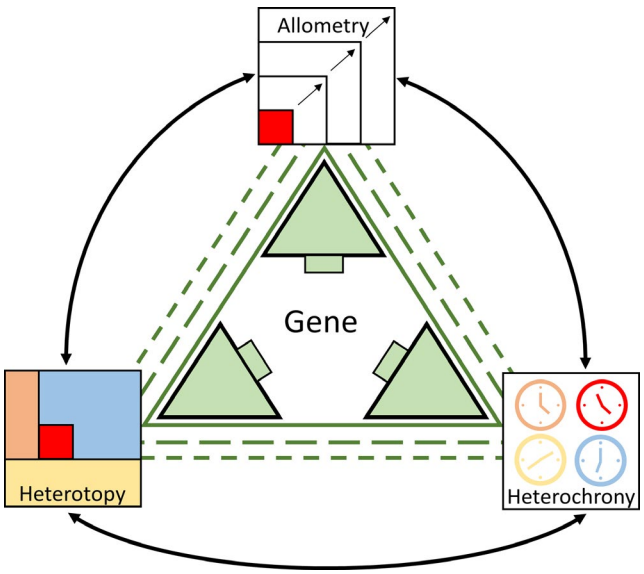

FIGURE 8 Diagrammatic representation of gene derived covariations of form manifested through heterochrony (timing), allometry (size) and heterotopy (location). As ontogeny progresses, these covariations lose coherence (broken green lines) and other sources (black lines) such as the competition for space between nearby enlarging structures (heterotopy-allometry) become more conspicuous

adult, spatially optimised, endpoints rather than along intraspecific prenatal ontogenies. The above paradigm also emphasises the importance of considering the protean mix of sources as well as the resulting patterns of covariation in studies of morphological integration and modularity over ontogenetic time (Klingenberg, 2008, 2014), and supports the case for explicitly recognising spatial-packing like covariations linked to heterotopy in the various theoretical frameworks that govern such studies and our current understanding of mammalian skull development.

ACKNOWLEDGEMENTS

The authors thank the many developers involved in creating and maintaining FEBio (www.febio.org), R (www.r-project.org), 3Dslicer (www.slicer.org) as well as MorphoJ (www.morphometrics.uk) and ImageJ (imagej.nih.gov). Without their support this research would not have been financially viable. The authors also thank the two reviewers for their comments and suggestions. Thanks to their input, the final version of this manuscript is a significant improvement on the original submitted.

CONFLICTS OF INTEREST

None declared.

DATA AVAILABILITY STATEMENT

The data that support the findings of this study are available from the corresponding author upon reasonable request.

ORCID

Nathan S. Jeffery https://orcid.org/0000-0001-5166-2029
Christopher L. Mendias https://orcid.org/0000-0002-2384-0171

REFERENCES

Amrhein, V., Greenland, S. & McShane, B. (2019) Comment: Retire statistical significance. *Nature*, 567, 305–307.

Anderson, P.S., Renaud, S. & Rayfield, E.J. (2014) Adaptive plasticity in the mouse mandible. *BMC Evolutionary Biology*, 14(1), 85.

Anthony, R. (1903) Introduction à l'étude expérimentale de la morphogénie. *Bulletins et Mémoires de la Société d'Anthropologie de Paris*, 4(1), 119–145.

Ateshian, G.A., Costa, K.D., Azeloglu, E.U., Morrison, B. & Hung, C.T. (2009) Continuum modeling of biological tissue growth by cell division, and alteration of intracellular osmolytes and extracellular fixed charge density. *Journal of biomechanical engineering*, 131(10), 101001.

Augustin, H., McGourty, K., Steinert, J.R., Cochemé, H.M., Adcott, J., Cabecinha, M. et al. (2017) Myostatin-like proteins regulate synaptic function and neuronal morphology. *Development*, 144(13), 2445–2455.

Bastir, M. & Rosas, A. (2016) Cranial base topology and basic trends in the facial evolution of Homo. *Journal of Human Evolution*, 91, 26–35.

Bastir, M., Rosas, A., Stringer, C., Cuétara, J.M., Kruszynski, R., Weber, G.W. et al. (2010) Effects of brain and facial size on basicranial form in human and primate evolution. *Journal of Human Evolution*, 58(5), 424–431.

Baverstock, H., Jeffery, N.S. & Cobb, S.N. (2013) The morphology of the mouse masticatory musculature. *Journal of Anatomy*, 223(1), 46–60.

Biegert, J. (1963). The evaluation of characteristics of the skull, hands and feet for primate taxonomy. In *Classification and human evolution* (Vol. 37, pp. 116–145). Aldine Chicago.

Bookstein, F.L. (2017) A newly noticed formula enforces fundamental limits on geometric morphometric analyses. *Evolutionary Biology*, 44(4), 522–541.

Bookstein, F.L. (2019) Pathologies of between-groups principal components analysis in geometric morphometrics. *Evolutionary Biology*, 46(4), 271–302.

Bourre, J.M., Morand, O., Chanez, C., Dumont, O. & Flexor, M.A. (1981) Influence of intrauterine malnutrition on brain development: alteration of myelination. *Neonatology*, 39(1–2), 96–99.

Byron, C.D., Hamrick, M.W. & Wingard, C.J. (2006) Alterations of temporalis muscle contractile force and histological content from the myostatin and Mdx deficient mouse. *Archives of Oral Biology*, 51(5), 396–405.

Cardini, A. (2019) Integration and modularity in procrustes shape data: Is there a risk of spurious results? *Evolutionary Biology*, 46(1), 90–105.

Cardini, A., O'Higgins, P. & Rohlf, F.J. (2019) Seeing distinct groups where there are none: Spurious patterns from between-group PCA. *Evolutionary Biology*, 46(4), 303–316.

Carneiro, I., González, T., López, M., Señarís, R., Devesa, J. & Arce, V.M. (2013) Myostatin expression is regulated by underfeeding and neonatal programming in rats. *Journal of physiology and biochemistry*, 69(1), 15–23.

Cox, P.G. & Jeffery, N. (2011) Reviewing the morphology of the jaw-closing musculature in squirrels, rats, and guinea pigs with contrast-enhanced microCT. *The Anatomical Record: Advances in Integrative Anatomy and Evolutionary Biology*, 294(6), 915–928.

Cray, J. Jr, Kneib, J., Vecchione, L., Byron, C., Cooper, G.M., Losee, J.E. et al. (2011) Masticatory hypermuscularity is not related to reduced cranial volume in myostatin-knockout mice. *The Anatomical Record: Advances in Integrative Anatomy and Evolutionary Biology*, 294(7), 1170–1177.

Deng, B., Zhang, F., Wen, J., Shen, W., Gao, Q., Peng, X. et al. (2020) The transcriptomes from two adipocyte progenitor cell types provide insight into the differential functions of MSTN. *Genomics*, 112(5), 3826–3836

Drake, A.G. & Klingenberg, C.P. (2008) The pace of morphological change: historical transformation of skull shape in St Bernard dogs. *Proceedings of the Royal Society B: Biological Sciences*, 275(1630), 71–76.

Dumoncel, J., Subsol, G., Durrleman, S., Bertrand, A., Jager, E., Oettlé, A.C. et al. (2020) Are endocasts reliable proxies for brains? A 3D quantitative comparison of the extant human brain and endocast. *Journal of Anatomy*, https://doi.org/10.1111/joa.13318.

Early, C.M., Iwaniuk, A.N., Ridgely, R.C. & Witmer, L.M. (2020) Endocast structures are reliable proxies for the sizes of corresponding regions of the brain in extant birds. *Journal of Anatomy*, 237(6), 1162–1176.

Edamoto, M., Kuroda, Y., Yoda, M., Kawaai, K. & Matsuo, K. (2019) Transpairing between osteoclasts and osteoblasts shapes the cranial base during development. *Scientific reports*, 9(1), 1–11.

Enlow, D.H. (1962) A study of the post-natal growth and remodeling of bone. *American Journal of Anatomy*, 110(2), 79–101.

Goswami, A., Binder, W.J., Meachen, J. & O'Keefe, F.R. (2015) The fossil record of phenotypic integration and modularity: A deep-time perspective on developmental and evolutionary dynamics. *Proceedings of the National Academy of Sciences*, 112(16), 4891–4896.

Gould, S.J. (2002) *The structure of evolutionary theory*. Harvard University Press.

Green, R.M., Fish, J.L., Young, N.M., Smith, F.J., Roberts, B., Dolan, K. et al. (2017) Developmental nonlinearity drives phenotypic robustness. *Nature communications*, 8(1), 1970.

Guo, T., Jou, W., Chanturiya, T., Portas, J., Gavrilova, O. & McPherron, A.C. (2009) Myostatin inhibition in muscle, but not adipose tissue,

decreases fat mass and improves insulin sensitivity. *PLoS One*, 4(3), e4937.

Hayashi, Y., Mikawa, S., Ogawa, C., Masumoto, K., Katou, F. & Sato, K. (2018) Myostatin expression in the adult rat central nervous system. *Journal of Chemical Neuroanatomy*, 94, 125–138.

Jarvis, D.A., Finney, C.R. & Griffiths, P.D. (2019) Normative volume measurements of the fetal intra-cranial compartments using 3D volume in utero MR imaging. *European Radiology*, 29(7), 3488–3495.

Jeffery, N. (2003) Brain expansion and comparative prenatal ontogeny of the non-hominoid primate cranial base. *Journal of human evolution*, 45(4), 263–284.

Jeffery, N. (2005) Cranial base angulation and growth of the human fetal pharynx. *The Anatomical Record Part A: Discoveries in Molecular, Cellular, and Evolutionary Biology: An Official Publication of the American Association of Anatomists*, 284(1), 491–499.

Jeffery, N., Davies, K., Köckenberger, W. & Williams, S. (2007) Craniofacial growth in fetal Tarsius bancanus: brains, eyes and nasal septa. *Journal of anatomy*, 210(6), 703–722.

Jeffery, N. & Mendias, C. (2014) Endocranial and masticatory muscle volumes in myostatin-deficient mice. *Royal Society Open Science*, 1(4), 140187.

Jeffery, N. & Spoor, F. (2002) Brain size and the human cranial base: a prenatal perspective. *American Journal of Physical Anthropology*, 118(4), 324.

Jeffery, N. & Spoor, F. (2004) Ossification and midline shape changes of the human fetal cranial base. *American Journal of Physical Anthropology*, 123(1), 78–90.

Jeffery, N.S., Stephenson, R.S., Gallagher, J.A., Jarvis, J.C. & Cox, P.G. (2011) Micro-computed tomography with iodine staining resolves the arrangement of muscle fibres. *Journal of Biomechanics*, 44(1), 189–192.

Kappers, C.A. (1932) The David Ferrier Lecture: On Some Correlations between Skull and Brain. Philosophical Transactions of the Royal Society of London. Series B, Containing Papers of a Biological Character, pp. 391–429.

Klingenberg, C.P. (2008) Morphological integration and developmental modularity. *Annual review of ecology, evolution, and systematics*, 39, 115–132.

Klingenberg, C.P. (2014) Studying morphological integration and modularity at multiple levels: concepts and analysis. *Philosophical Transactions of the Royal Society B: Biological Sciences*, 369(1649), 20130249.

Klingenberg, C.P. (2016) Size, shape, and form: concepts of allometry in geometric morphometrics. *Development genes and evolution*, 226(3), 113–137.

Kong, X., Yao, T., Zhou, P., Kazak, L., Tenen, D., Lyubetskaya, A. et al. (2018) Brown adipose tissue controls skeletal muscle function via the secretion of myostatin. *Cell Metabolism*, 28(4), 631–643.

Kyriakopoulou, V., Vatansever, D., Davidson, A., Patkee, P., Elkommos, S., Chew, A. et al. (2017) Normative biometry of the fetal brain using magnetic resonance imaging. *Brain Structure and Function*, 222(5), 2295–2307.

Lahti, D.C., Johnson, N.A., Ajie, B.C., Otto, S.P., Hendry, A.P., Blumstein, D.T. et al. (2009) Relaxed selection in the wild. *Trends in Ecology & Evolution*, 24(9), 487–496.

Laland, K.N., Uller, T., Feldman, M.W., Sterelny, K., Müller, G.B., Moczek, A. et al. (2015) The extended evolutionary synthesis: its structure, assumptions and predictions. *Proceedings of the Royal Society B: Biological Sciences*, 282(1813), 20151019.

Lee, C., Richtsmeier, J.T. & Kraft, R.H. (2019) A coupled reaction–diffusion–strain model predicts cranial vault formation in development and disease. *Biomechanics and Modeling in Mechanobiology*, 18(4), 1197–1211.

Lesciotto, K.M. & Richtsmeier, J.T. (2019) Craniofacial skeletal response to encephalization: How do we know what we think we know? *American Journal of Physical Anthropology*, 168, 27–46.

Lieberman, D.E., Ross, C.F. & Ravosa, M.J. (2000) The primate cranial base: ontogeny, function, and integration. *American Journal of Physical Anthropology: The Official Publication of the American Association of Physical Anthropologists*, 113(S31), 117–169.

Maas, S.A., Ellis, B.J., Ateshian, G.A. & Weiss, J.A. (2012) FEBio: finite elements for biomechanics. *Journal of Biomechanical Engineering*, 134(1), 011005.

McPherron, A.C. & Lee, S.J. (2002) Suppression of body fat accumulation in myostatin-deficient mice. *The Journal of Clinical Investigation*, 109(5), 595–601.

Mendias, C.L., Marcin, J.E., Calerdon, D.R. & Faulkner, J.A. (2006) Contractile properties of EDL and soleus muscles of myostatin-deficient mice. *Journal of Applied Physiology*, 101(3), 898–905.

Michejda, M. (1972) The role of basicranial synchondroses in flexure processes and ontogenetic development of the skull base. *American Journal of Physical Anthropology*, 37(1), 143–150.

Morand, O., Chanez, C., Masson, M., Dumont, O., Flexor, M.A., Baumann, N. et al. (1981) Intrauterine growth retardation (malnutrition by vascular ligation) induces modifications in fatty acid composition of neurons and oligodendrocytes. *Journal of Neurochemistry*, 37(4), 1057–1060.

Moss, M.L. & Young, R.W. (1960) A functional approach to craniology. *American Journal of Physical Anthropology*, 18(4), 281–292.

Mouisel, E., Relizani, K., Mille-Hamard, L., Denis, R., Hourdé, C., Agbulut, O. et al. (2014) Myostatin is a key mediator between energy metabolism and endurance capacity of skeletal muscle. *American Journal of Physiology-Regulatory, Integrative and Comparative Physiology*, 307(4), R444–R454.

Murren, C.J., Auld, J.R., Callahan, H., Ghalambor, C.K., Handelsman, C.A., Heskel, M.A. et al. (2015) Constraints on the evolution of phenotypic plasticity: limits and costs of phenotype and plasticity. *Heredity*, 115(4), 293.

Neaux, D., Gilissen, E., Coudyzer, W. & Guy, F. (2015) Integration between the face and the mandible of Pongo and the evolution of the craniofacial morphology of orangutans. *American Journal of Physical Anthropology*, 158(3), 475–486.

Neubauer, G. (1925). Experimentelle Untersuchungen über die Beeinflussung der Schädelform. Zeitschrift für Morphologie und Anthropologie, (H. 3), 411–442.

Oladipupo, L., Wood, B., Mano, N., Hughes, G., Reynolds, R., Vinyard, C. et al. (2020) Development of basicranium in cotton-top tamarin compared to the development of basicranium in bushbabies: Role of synchondroses and brain growth. *The FASEB Journal*, 34(S1), 1.

Ploquin, C., Chabi, B., Fouret, G., Vernus, B., Feillet-Coudray, C., Coudray, C. et al. (2012) Lack of myostatin alters intermyofibrillar mitochondria activity, unbalances redox status, and impairs tolerance to chronic repetitive contractions in muscle. *American Journal of Physiology-Endocrinology and Metabolism*, 302(8), E1000–E1008.

Ross, C.F. & Henneberg, M. (1995) Basicranial flexion, relative brain size and facial kyphosis in *Homo sapiens* and some fossil hominids. *American Journal of Physical Anthropology*, 98, 575–593.

Ross, C.F. & Kirk, E.C. (2007) Evolution of eye size and shape in primates. *Journal of Human Evolution*, 52(3), 294–313.

Ross, C.F. & Ravosa, M.J. (1993) Basicranial flexion, relative brain size, and facial kyphosis in nonhuman primates. *American Journal of Physical Anthropology*, 91, 305–324.

Schafer, M.J. & LeBrasseur, N.K. (2019) The influence of GDF11 on brain fate and function. *GeroScience*, 41(1), 1–11.

Singleton, M. (2013) Primate Cranial Diversity. *Nature Education Knowledge*, 4(12), 1.

Stedman, H.H., Kozyak, B.W., Nelson, A., Thesier, D.M., Su, L.T., Low, D.W. et al. (2004) Myosin gene mutation correlates with anatomical changes in the human lineage. *Nature*, 428(6981), 415.

Stewart, S., Darwood, A., Masouros, S., Higgins, C. & Ramasamy, A. (2020) Mechanotransduction in osteogenesis. *Bone & Joint Research*, 9(1), 1–14.

Vecchione, L., Byron, C., Cooper, G.M., Barbano, T., Hamrick, M.W., Sciote, J.J. et al. (2007) Craniofacial morphology in myostatin-deficient mice. *Journal of Dental Research*, 86(11), 1068–1072.

Vecchione, L., Miller, J., Byron, C., Cooper, G.M., Barbano, T., Cray, J. et al. (2010) Age-related changes in craniofacial morphology in GDF-8 (myostatin)-deficient mice. *The Anatomical Record: Advances in Integrative Anatomy and Evolutionary Biology*, 293(1), 32–41.

Veneziano, A., Meloro, C., Irish, J.D., Stringer, C., Profico, A. & De Groote, I. (2018) Neuromandibular integration in humans and chimpanzees: Implications for dental and mandibular reduction in Homo. *American Journal of Physical Anthropology*, 167(1), 84–96.

Vickerton, P., Jarvis, J. & Jeffery, N. (2013) Concentration-dependent specimen shrinkage in iodine-enhanced micro CT. *Journal of anatomy*, 223(2), 185–193.

Vincent, T.L. & Wann, A.K. (2019) Mechanoadaptation: articular cartilage through thick and thin. *The Journal of Physiology*, 597(5), 1271–1281.

Weidenreich, F. (1941) The brain and its role in the phylogenetic transformation of the human skull. *Transactions of the American Philosophical Society*, 31(5), 320–442.

Weiss, P. (1933) Functional adaptation and the role of ground substances in development. *The American Naturalist*, 67(711), 322–340.

Williams, S.H., Lozier, N.R., Montuelle, S.J. & de Lacalle, S. (2015) Effect of postnatal myostatin inhibition on bite mechanics in mice. *PLoS One*, 10(8), e0134854.

Wolff, J. (1893) Das gesetz der transformation der knochen. *DMW-Deutsche Medizinische Wochenschrift*, 19(47), 1222–1224.

Zelditch, M.L. & Fink, W.L. (1996) Heterochrony and heterotopy: Stability and innovation in the evolution of form. *Paleobiology*, 22(2), 241–254.

Zheng, J., Payne, J.L. & Wagner, A. (2019) Cryptic genetic variation accelerates evolution by opening access to diverse adaptive peaks. *Science*, 365(6451), 347–353.

Zollikofer, C.P.E., Bienvenu, T. & Ponce de León, M.S. (2017) Effects of cranial integration on hominid endocranial shape. *Journal of anatomy*, 230(1), 85–105.

Zollikofer, C.P.E. & Ponce De León, M.S. (2004) Kinematics of cranial ontogeny: heterotopy, heterochrony, and geometric morphometric analysis of growth models. *Journal of Experimental Zoology Part B: Molecular and Developmental Evolution*, 302(3), 322–340.

How to cite this article: Jeffery NS, Sarver DC, Mendias CL. Ontogenetic and *in silico* models of spatial-packing in the hypermuscular mouse skull. *J Anat*. 2021;238:1284–1295. https://doi.org/10.1111/joa.13393